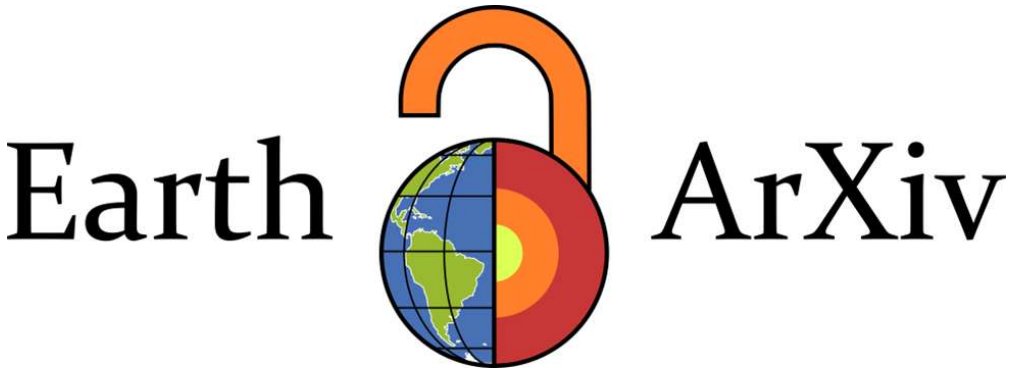


Embedding Probabilistic Pore Occupancy into Soil Hydraulic Models

Leonardo Inforsato
Independent researcher – inforsato.work@proton.me
https://orcid.org/0000-0001-9954-913X

This is a non-peer-reviewed preprint submitted to EarthArXiv.

This is a revised version of the manuscript first posted on Authorea (https://doi.org/10.22541/authorea.15011326/v1). The earlier Authorea rendering contains conversion errors in the numbering of equations, figures, and tables. This PDF reflects the revised manuscript submitted to *Hydrological Processes*.

This manuscript has been submitted for publication in *Hydrological Processes*. Please note the manuscript has yet to be formally accepted for publication. Subsequent versions of this manuscript may have slightly different content. If accepted, the final version of this manuscript will be available via the 'Peer-reviewed Publication DOI' link on the right-hand side of this webpage. Please feel free to contact any of the authors; we welcome feedback.

Embedding Probabilistic Pore Occupancy into Soil Hydraulic Models

Leonardo Inforsato

Independent researcher – inforsato.work@proton.me

https://orcid.org/0000-0001-9954-913X

Buckow, Brandenburg, Germany.

Abstract

Conventional soil hydraulic models describe unsaturated water retention and conductivity by assuming that water occupies the smallest pores, i.e., lower-energy pores. The author introduces a statistical pore occupancy framework to quantify the pore states by a pore distribution, retrieved from the retention function, allowing statistical inference of pore state conditions. The framework introduces a parameter b, which represents the water pore occupancy distribution, impacting the behavior of the retention and conductivity functions. The approach uses an effective energy formulation to facilitate the calculations, allowing direct integration into traditional soil-water dynamic simulators. As a second step, a back transformation is introduced for a direct physical interpretation of the pore-filling condition, leading to the probability of pores being filled or not filled with water. The framework introduces a modified closed-form formulation of the Van Genuchten-Mualem model. The new model can quantify hysteretic behavior of the retention function and simultaneously predict the hydraulic conductivity behavior. Root mean square differences (RMSD) ranged from 0.007 to 0.021 $\mathrm{m}^3\ \mathrm{m}^{-3}$, for the retention data, predicting both drying and wetting experiment scenarios; and from 0.117 to 0.216 for the conductivity, expressed as $\log_{10}(K)$. The embedded statistical mechanic can also assist in quantifying the solute transport. The respective shapes of the solute breakthrough curves (BTC) were reproduced, leading to a calibration RMSD of 0.018 and 0.016 [–]. A discussion regarding the back-transformation showed how the framework can be used to infer the configuration of pores filled with water in the soil, considering the model assumptions.

1. INTRODUCTION

Water is the most restrictive resource in the soil for plants. Water is essential to the physical and chemical processes in plants, acting directly over solutes transport to the roots, as result of its solvent properties. Consequently, water availability influences the development of the plant at multiple phenological stages by restricting photosynthesis and respiration, influencing the transport of nutrients to the rhizosphere, or even making them inaccessible by nutrient leaching. For quantitative assessment of the water state in soil, the most commonly used soil-water continuum approach is derived from the mass conservation law: the *Richards equation-based models*, RE (Celia et al., 1990; Vereecken et al., 2016). Compared with other quantitative approaches for soil-water assessments, like the tipping bucket model, TB (Emerman, 1995; Inforsato and De Jong Van Lier, 2021), the RE models have the capability of describing the water state in the soil continuously.

As a consequence, the RE approach is the most used approach for soil-water studies requiring detailed description of the water state in the soil. On the other hand, the RE approach generally requires more parameters than TB, thus requiring more experimental data (De Jong Van Lier, 2017; Turek et al., 2022).

Another category is the data-driven (DD) models for soil-water assessments. The DD model category uses machine learning (ML) methods to fit parameters to measured data; these parameters commonly lack a direct physical interpretation or dimension. The resulting ML model has a relatively high number of parameters, in comparison to other process-based models (RE and TB). These models have become increasingly popular due to some desirable features, including: the possibility to represent complex behavior, strong prediction of non-linear relationships, and simultaneous interaction with multiple heterogeneous variables (Minasny et al., 2024; Zhang et al., 2026). The DD models are known for their *black-box* characteristic (Padarian et al., 2020), i.e., models in which the input and output relationship cannot be readily interpreted in physical terms. Black-box DD models for soil-water flux prediction rely on the accuracy and size of the dataset used for model fitting. To address the black-box characteristics, ad hoc strategies are used, the most common being explainable machine learning, or XAI (Ryo, 2022). Nevertheless, XAI can only partially improve the model interpretability (Padarian et al., 2020).

Multiple soil-water relationship models are available for RE use: Groenevelt–Grant (Grant et al., 2010; Groenevelt and Grant, 2004), Fredlund-Xing (Fredlund and Xing, 1994), Childs and Collis-George (Childs and Collis-George, 1950). The most used is the Van Genuchten retention function with the Mualem capillary bundle model (Mualem, 1976; Van Genuchten, 1980), referred to in this article as VG. Some approaches adapt a specific model to predict behavior originally unaddressed by the original soil-water models (Inforsato et al., 2020). Two of these unaddressed phenomena are: hysteretic behavior observed in experimental data for the retention function, and preferential flow. The most commonly used approaches to assess hysteresis and preferential flow are multi-modal approaches. Multi-modal approaches are characterized by two or more domain classes acting simultaneously on the same outcome; e.g., for preferential flow: Durner's multi-modal VG (Durner, 1994), or dual-permeability (Gerke and Van Genuchten, 1993); and for hysteretic retention function: scanning-curve models from Kool and Parker (1987), and from Mualem (1974).

Xu and Louge (2015) applied a statistical physics (SP) framework to soil-water retention using an Ising formulation. In this model, each pore is assumed to be completely filled either with air or with water, while liquid films are neglected. The porous medium is represented by monodisperse solid spheres arranged in a random packing, so that positional disorder generates a distribution of pore and neck geometries. From this geometrical disorder and the collective interactions among neighboring pores, the model predicts different drying and wetting retention energies and therefore hysteresis. More recently, Rigon (2026) developed a SP framework in which pore-class occupancy is treated as a dynamical variable, with non-equilibrium evolution governed by pore-network connectivity, accessibility, and inter-pore redistribution. Zehe et al. (2021) connected free energy, entropy, and preferential flow. More generally, Hansen et al. (2023) developed a Jaynes-based (Jaynes, 1957) SP framework for immiscible two-phase flow in porous media, introducing configurational entropy and thermodynamic variables at the Darcy scale.

Visintin (1994) defines hysteresis as a rate-independent memory effect. In soil physics, SP provides a natural framework for describing hysteretic soil-water behavior, because hysteresis is intrinsically history-dependent: at the same matric potential, the corresponding water content may differ depending on the previous water state. At the pore scale, such path dependence can arise from connectivity constraints, local capillary energy barriers, and irreversible dissipation during fluid redistribution. These mechanisms may act independently and/or jointly to determine the macroscopic hysteretic characteristic (Lu and Khorshidi, 2015; Or and Tuller, 2023; Xu and Louge, 2015).

Hysteresis is studied across multiple areas of physics, including soil physics. However, SP-based descriptions of hysteresis are generally not directly connected to the constitutive models traditionally used to describe soil-water retention and hydraulic conductivity. This article introduces an SP framework that is explicitly coupled to a widely used soil-water relationship model. A new coupling parameter is incorporated into the retention and conductivity functions to quantify the contribution of the probabilistic pore-filling mechanism. The framework is used to evaluate how quasi-equilibrium pore-energy states change the macroscopic hydraulic experimental observations. These modifications are associated with hysteresis and preferential-flow behavior. The introduced model does not focus on increasing the predictive accuracy, but on quantitatively imbuing a new physical mechanism in traditional models. To demonstrate the framework's potential, the author chose VG for a more in-depth implementation and discussion.

The introduced SP formulation relies on four fundamental concepts: the ensemble description, the energy-scaling parameter β, entropy, and the Boltzmann distribution together with its partition function. These concepts are briefly introduced here, a more extensive discussion can be found in standard SP texts like Blundell and Blundell, (2009) and Schroeder, (2021).

Ensemble: a large collection of hypothetical copies of a system, each representing one possible microstate consistent with the imposed macroscopic constraints. Specifically, a canonical ensemble is an ensemble in which the number of particles, volume, and temperature are fixed.

Energy-scaling parameter β: in thermodynamics, the parameter β [J^{-1}] is defined as $\beta = \left(k_B \cdot T\right)^{-1}$, (where k_b is the Boltzmann constant [$\mathrm{J\ K}^{-1}$], and T is the temperature [K]), but this definition cannot be generalized to all systems. A more general definition for the parameter β is provided by Jaynes, (1957), defining β as a Lagrange multiplier for the entropy maximization, subject to constraints of mean energy and probabilities summing 1, or 100%.

Entropy: before defining entropy, we define the multiplicity, Ω [–], as the number of accessible microstates corresponding to a given macrostate. For equally probable microstates, the Ω relates to the Boltzmann entropy, S_B [$\mathrm{J\ K}^{-1}$] as

$$S_B = k_B \ln\left(\Omega\right) \qquad \text{(Eq. 1)}$$

More generally, if the accessible microstates have probability of occurrence P_i, the dimensionless entropy, S_e [–], becomes

$$S_e = -\sum_i P_i \ln\left(P_i\right) \qquad \text{(Eq. 2)}$$

where P_i is the probability of microstate i. The corresponding dimensionless entropy is $S_e = entropy / k_B$. This formulation is known as Gibbs entropy.

Boltzmann distribution: in the maximum entropy formulation, the probability P_i occupying an energy state e_i [J], is proportional to the Boltzmann factor,

$$P_i(e_i) \propto \exp(-\beta \cdot e_i) \quad \text{(Eq. 3)}$$

Normalization of this proportion yields the Boltzmann distribution.

The development of the model is split into seven sections.

(i) In Section 2.1, the relationships between pore energy and other properties, including pore geometry (radius and volume) and pressure head, are defined. This section establishes the properties of the microstates.

(ii) In Section 2.2, the general SP formulation of the pore-occupancy model is defined.

(iii) In Section 2.3, the SP formulation is incorporated into the VG soil-water retention model (Van Genuchten, 1980). An effective pore-energy representation is introduced to obtain a closed-form retention function and the corresponding effective coupling parameter b.

(iv) In Section 2.4, the resulting retention formulation is incorporated into the Mualem, (1976) capillary-bundle model to derive the corresponding hydraulic conductivity function.

(v) In Section 2.5, the effective coupling parameter b is back-transformed to a physical-energy representation, allowing physical interpretability and the corresponding physical pore-occupancy distribution to be quantified.

(vi) In Section 2.6, the entropy associated with the proposed statistical-physical formulation is defined.

(vii) In the Appendix, the SP framework is additionally applied to the breakthrough curve (BTC) for solute transport and to the Brooks-Corey retention function.

2. MATERIAL AND METHODOLOGY

2.1. Pore energy distribution function

The pore energy distribution is defined based on the cylindrical pore volume (Nimmo et al., 2007). Definition of the pore shape: cylindrical pore volume, V_p [m^3],

$$V_p = \pi r^2 \cdot l \quad \text{(Eq. 4)}$$

l = length of the cylinder [m]

r = radius of the cylinder [m]

Young-Laplace equation for a capillary cylinder (Siqveland and Skjaeveland, 2021)

$$\Delta P = -\frac{2 \cdot \gamma \cdot \cos \mu}{r} \quad \text{(Eq. 5)}$$

ΔP = Pressure difference between the water-air interface in the cylinder [$\mathrm{N\ m^{-2}}$]

γ = interfacial tension between water and air [$\mathrm{N\ m^{-1}}$]

μ = contact angle between the water and the solid [–]

The relationship between P and the capillary pressure head, ψ [m], is defined as

$$\Delta P = \psi \cdot \rho_w \cdot g \quad \text{(Eq. 6)}$$

g = gravity acceleration [$\mathrm{m\ s^{-2}}$]

ρ_w = water density [$\mathrm{kg\ m^{-3}}$]

We define the negative of the pressure head as a function of the radius,

$$h(r) = -\psi(r) = \frac{2 \cdot \gamma \cdot \cos \mu}{\rho_w \cdot g \cdot r} \quad \text{(Eq. 7)}$$

The energy associated with the capillary pressure head, e_w [J], is defined as

$$e_w = m_w \cdot g \cdot h \quad \text{(Eq. 8)}$$

m_w = water mass [kg]

Combining the Eq. 7 with Eq. 8, we define the relationship between e_w and r,

$$e_w(r) = \frac{2 \cdot \gamma \cdot \cos \mu \cdot m_w}{\rho_w \cdot r} \quad \text{(Eq. 9)}$$

For the proposed model, it is convenient to define a fixed elementary water volume, V_0 [$\mathrm{m^3}$], which is treated as a discrete water particle for model development, leading to a particle model (Zehe et al., 2019; Zehe and Jackisch, 2016).

$$V_0 = \pi r_0^2 \cdot l_0 \quad \text{(Eq. 10)}$$

l_0 = minimum length of the cylinder pore [m]

r_0 = minimum radius of the cylinder pore [m]

Using $m_w = \rho_w V_0$, the energy pore radius ratio becomes

$$e_w(r) = \frac{2 \cdot \gamma \cdot \cos \mu \cdot V_0}{r} \quad \text{(Eq. 11)}$$

As a consequence of the elementary volume discretization, each pore state is represented by a binary occupation variable. A pore state is either occupied by the water volume V_0, or it is vacant. The model does not allow a fraction of occupied states.

The water capacity, $C(h)$ [$\mathrm{m^{-1}}$], is defined as the negative derivative of the retention function, $\theta(h)$ [$\mathrm{m^3\ m^{-3}}$], with respect to the capillary pressure head

$$C(h) = -\frac{d\theta}{dh} \quad \text{with } C(h) \geq 0\ \mathrm{m^{-1}} \quad \text{(Eq. 12)}$$

The pore-size distribution, f_p [m^{-1}], is defined as

$$f_p = \left|\frac{d\theta}{dr}\right| \quad \text{(Eq. 13)}$$

Under the capillary bundle assumption, $C(h)$ is related to the pore-size distribution, f_p (with respect to the radius) through

$$f_p(r) = C(h)\left|\frac{dh}{dr}\right| \quad \text{(Eq. 14)}$$

Since both $h(r)$ and $e(r)$, monotonically decrease with respect to r, we define the capacity functions as positive; the same modulus implementation is repeated for the distributions defined.

The same Eq. 14 is also found under slightly different formulations in Zheng et al. (2020).

The function $f_p(r)$, converted from radius space to energy, using the chain rule, becomes

$$f_E(e_w) = f_p(r(e_w))\left|\frac{dr}{de_w}\right| = \left|-\frac{d\theta}{dh}\frac{dh}{dr}\frac{dr}{de_w}\right| \quad \text{(Eq. 15)}$$

From Eq. 7, the derivative of h with respect to r becomes

$$\frac{dh}{dr} = -\frac{2\cdot\gamma\cdot\cos\mu}{\rho_w\cdot g\cdot r^2} \quad \text{(Eq. 16)}$$

Fixing the water volume to V_0 and using Eq. 9, we can calculate

$$\frac{dr}{de_w} = -\frac{r^2}{2\cdot\gamma\cdot\cos\mu\cdot V_0} \quad \text{(Eq. 17)}$$

Combining Eq. 16 and Eq. 17, we achieve the constant,

$$\frac{dh}{dr}\frac{dr}{de_w} = \frac{1}{\rho_w\cdot g\cdot V_0} \quad \text{(Eq. 18)}$$

Finally, the pore-energy density function derived from the retention function becomes

$$f_E(e_w) = C(h(e_w))\frac{1}{\rho_w\cdot g\cdot V_0} \quad \text{(Eq. 19)}$$

2.2. Boltzmann probability distribution for the pore model

At equilibrium, the probability density in function of e_w, $P(e_w)$, using the pore-energy distribution $f_E(e_w)$, (Eq. 19) is defined as

$$P(e_w) = \frac{f_E(e_w)\cdot\exp(-\beta\cdot e_w)}{Z} \quad \text{(Eq. 20)}$$

where

$$Z = \int_{e_{sat}}^{e_0} f_E(e_w)\cdot\exp(-\beta\cdot e_w)\, de_w \quad \text{(Eq. 21)}$$

Z = normalization factor [–].

β = inverse energy scale parameter [J^{-1}]

e_{sat} = energy associated with the pore with maximum radius [J]

e_0 = energy associated with the pore with minimum radius [J]

The Eq. 20 is the probability density over the filled pore classes, as a function of its capillary energy e_w. $P(e_w)$ has unit J^{-1}, while integrating over an interval gives the probability mass assigned to those classes, with no unit, [–].

In classical thermodynamics, β is defined as a constant with value $\beta = 1/(k_B \cdot T)$, where k_B is the Boltzmann constant and T [K] is the temperature. In the present pore-scale formulation, β is treated as a parameter for the effective inverse energy scale [J^{-1}]. The relevant energy states are associated with the capillary pore-scale configuration, instead of molecular thermal energy oscillations. Effective values for β has been introduced in granular statistical mechanics, where the volume-based compactivity (or its inverse) is inferred from the state distribution, instead of the actual temperature (Puckett and Daniels, 2013; Yuan et al., 2021). In particular, in the maximum entropy formulation proposed by Jaynes (1957), β is interpreted as a Lagrange multiplier.

2.3. Van Genuchten Retention function adaptation

The VG retention function is defined as

$$\Theta_{VG}(h) = \left[1 + (\alpha h)^n\right]^{-m} \quad \text{(Eq. 22)}$$

where

$$\Theta(\theta) = \frac{\theta - \theta_r}{\theta_s - \theta_r} \quad \text{(Eq. 23)}$$

θ = water content [$m^3\ m^{-3}$]

θ_r = residual water content [$m^3\ m^{-3}$]

θ_s = saturated water content [$m^3\ m^{-3}$]

n = fitting parameter [–]

m = fitting parameter [–]

α = fitting parameter [m^{-1}]

h_{VG} = pressure head magnitude [m]

When $\Theta = 1 \Rightarrow h = 0$ m, and when $\Theta = 0 \Rightarrow h \to \infty$ m.

The $C(h)$ from Eq. 12, for the VG function becomes

$$C_{VG}(h) = -\frac{d\theta}{dh} = (\theta_s - \theta_r)\, mn\alpha (\alpha h)^{n-1} \left[1 + (\alpha h)^n\right]^{-m-1} \quad \text{(Eq. 24)}$$

We can also calculate the pore-energy distribution as a function of h using VG. Modifying Eq. 8 we achieve the expression for energy as a function of the magnitude of the pressure head

$$e_w(h) = h \cdot \rho_w \cdot V_0 \cdot g \quad \text{(Eq. 25)}$$

The derivative is

$$\frac{de_w}{dh} = \rho_w \cdot V_0 \cdot g \quad \text{(Eq. 26)}$$

Combining it with Eq. 19 and Eq. 20, we have

$$P^*_{VG}(h,\beta) = \frac{C_{VG}(h)\exp(-b\cdot\alpha\cdot h)}{\int_0^\infty C_{VG}(h)\exp(-b\cdot\alpha\cdot h)\,dh} \quad \text{(Eq. 27)}$$

Leading to

$$\Theta^*_{VG}(h,\beta) = \frac{\int_h^\infty C_{VG}(h)\exp(-b\cdot\alpha\cdot h)\,dh}{\int_0^\infty C_{VG}(h)\exp(-b\cdot\alpha\cdot h)\,dh} \quad \text{(Eq. 28)}$$

With the restriction

$$b > 0 \quad \text{(Eq. 29)}$$

The Eq. 28 is the saturation as a function of h, using b as a parameter. Unfortunately, using the linear relationship between the energy and h results in a model which requires numerical integration to solve. To address this issue, the author proposes a specific energy definition, which is algebraically compatible with the VG retention model. Starting from the energy model in the exponential form (Eq. 20), combined with the linear energy in relation to h (Eq. 25) we can write the energy relationship as

$$\exp(-\beta\cdot e_w) = \exp(-b\alpha h) \quad \text{(Eq. 30)}$$

With b as

$$b = \frac{\beta\cdot\rho_w\cdot V_0\cdot g}{\alpha} \quad \text{(Eq. 31)}$$

The proposed energy relationship, matching the VG retention model algebraically, is

$$\exp(-\beta\cdot e_{eff}) = \exp\left(-b\cdot\ln\left(\left[1+(\alpha h)^n\right]\right)\right) \quad \text{(Eq. 32)}$$

Here, the e_{eff} [J] is the effective energy used as a function of the pressure head. The equation keeps interesting properties of Eq. 30, both are continuous and smooth monotonically increasing functions; both have zero energy at $h = 0$ m, both equations are invertible on the $e_{eff} \leftrightarrow h \leftrightarrow e_w$ relationship.

The equation Eq. 32 leads to the following derivative with respect to h

$$\frac{de_{eff}}{dh} = \rho_w\cdot V_0\cdot g\cdot\frac{n(\alpha h)^{n-1}}{1+(\alpha h)^n} \quad \text{(Eq. 33)}$$

combining it with Eq. 19 and Eq. 20,

$$P_{VG}(h,\beta)=\frac{f_{eff}\left(e_{eff}(h)\right)\cdot\exp\left(-\beta\cdot e_{eff}(h)\right)\rho_w\cdot V_0\cdot g\cdot\dfrac{n(\alpha h)^{n-1}}{1+(\alpha h)^n}}{Z_{VG}} \quad \text{(Eq. 34)}$$

Where f_{eff} is the density function

$$f_{eff}\left(e_{eff}(h)\right)=\frac{C_{VG}(h)}{(\theta_s-\theta_r)}\frac{dh}{de_{eff}} \quad \text{(Eq. 35)}$$

With the Z_{VG} as the normalization factor. Using the definition of m and b as

$$m=1-\frac{1}{n},\qquad b=\frac{\beta\cdot\rho_w\cdot V_0\cdot g}{\alpha} \quad \text{(Eq. 36)}$$

We can write

$$f_{eff}\left(e_{eff}(h)\right)\frac{de_{eff}}{dh}=(n-1)\alpha^n h^{n-1}\left[1+(\alpha h)^n\right]^{-\left(2-\frac{1}{n}\right)} \quad \text{(Eq. 37)}$$

Now, solving the Z_{VG},

$$Z_{VG}=\int_0^\infty (n-1)\alpha^n h^{n-1}\left[1+(\alpha h)^n\right]^{-\left(2-\frac{1}{n}+b\right)}dh=\frac{n-1}{n(1+b)-1} \quad \text{(Eq. 38)}$$

Substituting into Eq. 34, the P_{VG} becomes

$$P_{VG}(h,\mathrm{b})=\alpha^n\left[n(1+b)-1\right]h^{n-1}\left[1+(\alpha h)^n\right]^{-\left(2-\frac{1}{n}+b\right)} \quad \text{(Eq. 39)}$$

Integrating the P_{VG} with respect to h, we obtain the saturation, Θ [–],

$$\Theta(h,\beta)=\int_h^\infty P_{VG}(h,\beta)\,dh \quad \text{(Eq. 40)}$$

Eq. 40 expresses the effective saturation as the probability mass assigned to states above the pressure-head threshold h. Equivalently, it is the ensemble average of a binary indicator that equals 1 for states above the threshold and 0 otherwise. The parameter b modifies the statistical weighting of these states and therefore the saturation associated with a given macroscopic pressure head. Integrating Eq. 40 results in

$$\Theta(h,b)=\left[1+(\alpha h)^n\right]^{-1-b+\frac{1}{n}} \quad \text{(Eq. 41)}$$

With restrictions

$$\alpha>0,\quad n>1,\quad n(1+b)-1>0 \quad \text{(Eq. 42)}$$

Resulting in the retention function

$$\theta(h,b)=\theta_r+(\theta_s-\theta_r)\left[1+(\alpha h)^n\right]^{-1-b+\frac{1}{n}} \quad \text{(Eq. 43)}$$

Note that when $b=0$, the retention function becomes the original VG retention function.

2.4. Conductivity model under Mualem's assumption

The Mualem (1976) capillary bundle model is defined as

$$K_{rel} = \Theta^{\lambda}\left[\frac{\int_0^{\Theta}\frac{1}{h(\Theta)}\,d\Theta}{\int_0^{1}\frac{1}{h(\Theta)}\,d\Theta}\right]^2 \quad \text{(Eq. 44)}$$

The inverse of the saturation function of the modified VG model (inverse of Eq. 41), is

$$h(\Theta, b) = \frac{1}{\alpha}\left[\Theta^{-\frac{n}{n(1+b)-1}} - 1\right]^{1/n} \quad \text{(Eq. 45)}$$

The substitution of Eq. 45 into Eq. 44 admits analytical representation, using the regularized incomplete beta function, $I_{\Theta^{n/[n(1+b)-1]}}$ [–] (Didonato & Morris, 1992). Solving the integral, the relative hydraulic conductivity results in

$$K_{rel} = \Theta^{\lambda}\left[I_{\Theta^{\frac{n}{n(1+b)-1}}}\left(1+b, \frac{n-1}{n}\right)\right]^2 \quad \text{(Eq. 46)}$$

where

$$I_{\Theta^{\frac{n}{n(1+b)-1}}}\left(1+b, \frac{n-1}{n}\right) = \frac{\int_0^{\Theta^{\frac{n}{n(1+b)-1}}} t^b\left(1-t\right)^{-1/n}\,dt}{\int_0^{1} t^b\left(1-t\right)^{-1/n}\,dt} \quad \text{(Eq. 47)}$$

The conductivity equation, Eq. 46, is mathematically equivalent to the general Van Genuchten-Mualem conductivity formulation discussed by Dourado Neto et al. (2011).

For arbitrary n, b, and Θ, the regularized incomplete beta function generally does not reduce to an elementary expression, and is evaluated numerically. To obtain an analytical conductivity function, the following approximation is proposed,

$$I_{\Theta^{\frac{n}{n(1+b)-1}}}\left(1+b, \frac{n-1}{n}\right) \approx 1 - \left(1 - \Theta^{\frac{n(1+b)}{n(1+b)-1}}\right)^{\frac{n-1}{n}} \quad \text{(Eq. 48)}$$

Substituting into Eq. 46 leads to

$$K_{rel} \approx \Theta^{\lambda}\left[1 - \left(1 - \Theta^{\frac{n(1+b)}{n(1+b)-1}}\right)^{\frac{n-1}{n}}\right]^2 \quad \text{(Eq. 49)}$$

Eq. 49 is the approximated K_{rel} function with the b parameter embedded. Eq. 46 is the K_{rel} function formulated with the incomplete beta function.

2.5. Back–transformation of effective parameter b to physical parameter b_{phys}

The parameter b formulated over the e_{eff} energy is convenient to achieve a closed-form formulation, allowing direct use and implementation in traditional soil dynamics simulators. Although e_w and e_{eff} have multiple shared properties, they are not the same, leading to a transformation from b to the physical b parameter, $b_{phys}(e_w)$. In this section,

we propose a conversion to go from $b \rightarrow b_{phys}$, to allow physical quantification of the pore occupancy. From Eq. 32, we can manipulate to

$$b_{phys}\left(e_w\right)\frac{\alpha \cdot e_w}{\rho_w \cdot V_0 \cdot g} = b \cdot \ln\left[1+\left(\frac{\alpha \cdot e_w}{\rho_w \cdot V_0 \cdot g}\right)^n\right] \quad \text{(Eq. 50)}$$

Another option to evaluate the coefficient in practice is to express b_{phys} as a function of saturation (Θ). Starting from Eq. 41, we write

$$\Theta\left(h,b\right) = \left[1+\left(\alpha h\right)^n\right]^{-1-b+\frac{1}{n}} \quad \text{(Eq. 51)}$$

Therefore

$$\alpha h = \left[\Theta\left(h,b\right)^{-\frac{n}{n(1+b)-1}} - 1\right]^{1/n} \quad \text{(Eq. 52)}$$

Substituting into Eq. 50,

$$b_{phys}\left(\Theta\right) = b \cdot \frac{\frac{n\ln\left[\Theta\right]}{1-n\left(1+b\right)}}{\left[\Theta^{\frac{n}{1-n-nb}} - 1\right]^{1/n}} \quad \text{(Eq. 53)}$$

This formulation maps b_{phys} over the saturation degree.

A natural next step is to calculate the probability of pore occupancy, based on h, for the VG model. Starting from the Boltzmann probability density in Eq. 20, we express the probability in physical pore-energy

$$P\left(e_w\right) \propto f_E\left(e_w\right) \cdot \exp\left(-b_{phys}\left(e_w\right) \cdot \frac{\alpha \cdot e_w}{\rho_w \cdot V_0 \cdot g}\right) \quad \text{(Eq. 54)}$$

Leading to

$$P\left(e_w\right) \propto f_E\left(e_w\right)\left[1+\left(\frac{\alpha \cdot e_w}{\rho_w \cdot V_0 \cdot g}\right)^n\right]^{-b} \quad \text{(Eq. 55)}$$

From Eq. 19 and Eq. 26, we have

$$f_E\left(e_w\right) = \frac{C_{VG}\left(h\left(e_w\right)\right)}{\rho_w \cdot g \cdot V_0} \quad , \quad de_w = \rho_w \cdot V_0 \cdot g \;\; dh \quad \text{(Eq. 56)}$$

Leading to the probability as a function of h,

$$P_{VG}\left(h,b\right) = \frac{C_{VG}\left(h\right)\left[1+\left(\alpha h\right)^n\right]^{-b}}{\int_0^\infty C_{VG}\left(h\right)\left[1+\left(\alpha h\right)^n\right]^{-b} dh} \quad \text{(Eq. 57)}$$

With $P_{VG}(h,b)$ in $[\mathrm{m}^{-1}]$. For the VG model, the probability density of pore occupancy with respect to h, becomes,

$$P_{VG}\left(h,b\right)=\left[n\left(1+b\right)-1\right]\alpha\left(\alpha h\right)^{n-1}\left[1+\left(\alpha h\right)^{n}\right]^{-2-b+1/n} \quad \text{(Eq. 58)}$$

The $P_{VG}(h,b)$ is the probability density over the filled pore classes, as a function of h.

2.6. The entropy of filled and unfilled pores

The probabilistic description of pore occupancy also allows the configurational entropy associated with water distribution to be evaluated. This quantity describes the multiplicity of possible arrangements of occupied and vacant sites under specified macroscopic conditions. For an idealized system of N equivalent, independent occupation sites, the probabilities of a site being occupied by water or remaining vacant are defined as $P_w=\Theta$ and $P_a=1-\Theta$, respectively. Substituting these probabilities into the Gibbs entropy expression (Eq. 2) gives

$$S_{occ}=-N\left[\Theta\ln\Theta+\left(1-\Theta\right)\ln\left(1-\Theta\right)\right] \quad \text{(Eq. 59)}$$

Where S_{occ} [–] is the configurational entropy of filled/unfilled pores. The stationary condition for S_{occ} [–] as a function of h, results in

$$\frac{dS_{occ}}{dh}=N\ln\left(\frac{1-\Theta\left(h\right)}{\Theta\left(h\right)}\right)\frac{d\Theta\left(h\right)}{dh}=0 \quad \text{(Eq. 60)}$$

The configurational entropy in Eq. 59 reaches its maximum at $\Theta=0.5$, reflecting the greatest multiplicity of arrangements of filled and unfilled pores, under the assumed model. This maximum is a property of the statistical representation and does not, by itself, imply that soil water evolves toward half saturation. The entropy quantifies the configurational contribution associated with the coexistence of filled and unfilled pores, without requiring the microscopic mechanisms governing their occupancy to be specified. Its role is therefore to characterize pore occupancy within the proposed framework, while the physically accessible configurations remain subject to water-content and energetic constraints.

2.7. Suggested framework process flow using b parameter

Figure 1 illustrates the proposed workflow for applying the SP model. The parameter b is fitted from macroscopic measurements and can be incorporated into Richards' equation-based simulators for water flow and solute transport. When a physical interpretation of pore occupancy is needed, the fitted parameter can be back-transformed to obtain the corresponding probability distribution.

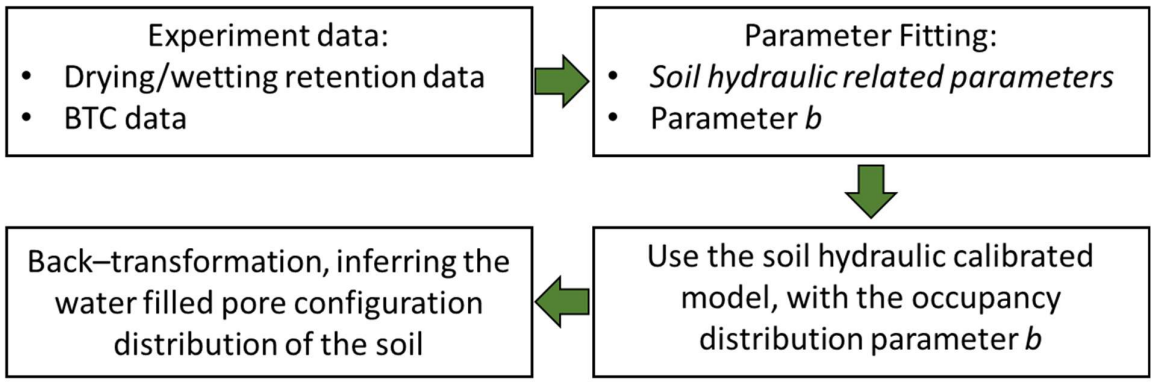


Figure 1 – Proposed process flow framework for the introduced statistical physical model.

2.8. Testing and discussing the model

We define the evaluation processes for the proposed probabilistic model over different scenarios where the probabilistic characteristics of the model might be impactful, including for hysteresis and solute transport analysis. All the fitting processes described in this section were performed by minimizing the objective function, Of, described as

$$Of = \sum_{i=i}^{k} \left(Y_i - \hat{Y}_i \right)^2 \quad \text{(Eq. 61)}$$

Y = target value

$\hat{Y}$ = predicted value

This general approach is named Least Squares, which is a common approach to fit both the retention and conductivity functions simultaneously (Inforsato et al., 2020; Köhne et al., 2002). The specific algorithm used for the fitting process is the Trust Region Reflective algorithm (Branch et al., 1999). The implementation was done using the SciPy library, version 1.18.0.

The main metric used to compare the differences between target and predicted values is the RMSD (root mean squared difference).

2.8.1. Evaluation of the approximations and energy redefinition involved in the model definition

The proposed model for the retention and conductivity functions relies on one main approximation and the redefinition of the energy:

(i) the energy conversion from e_w, to the exponential form, e_{eff} (Eq. 25 and Eq. 32, respectively);

(ii) the regularized incomplete beta function approximation (Eq. 47).

To evaluate energy redefinition (i), the author compares the values of the saturation function, Θ, using the effective energy formulation (Eq. 41), and the equivalent equation

using numerical solution, with e_w (Eq. 28). The metric to quantify the distance between both scenarios is the RMSD.

The second test (ii) is a comparison of the conductivity function, comparing Eq. 46 with Eq. 49. To quantify the difference between both approaches, the RMSD metric is also established.

For the approximation and energy redefinition tests, the author selected 3 standard soil datasets extracted from the Rosetta model (Schaap et al., 2001): Loamy Sand, Silt Loam, and Silty Clay, according to the 12 USDA soil texture classification. The parameters are available in Table 1. All the comparisons are realized over the domain:

$$h \in \left[10^{-3}, 10^{3}\right] \text{ m} \qquad \text{(Eq. 62)}$$

A thousand points evenly spaced on a logarithmic scale (base 10) are sampled for the tests and RMSD calculation.

Table 1– Selected soil texture classes with respective Van Genuchten-Mualem model parameters

USDA texture	θ_r	θ_s	$\alpha[\text{m}^{-1}]$	n	K_s [m s^{-1}]
Loamy sand	0.049	0.390	3.475	1.746	$1.218 \cdot 10^{-5}$
Silt loam	0.065	0.439	0.506	1.663	$2.111 \cdot 10^{-6}$
Silty clay	0.111	0.481	1.622	1.321	$1.113 \cdot 10^{-6}$

2.8.2. Testing the Van Genuchten retention and conductivity functions: comparing $b = 0$ and the $b > 0$

To evaluate the capability of predicting the retention function hysteresis, the author uses point data datasets from UNSODA (Nemes et al., n.d.), soil datasets: 1300, 2020, 4870, with respect to soil texture classes: Sandy clay loam, Clay loam, and Silt loam; and from the Mualem catalogue (Mualem, 1976a): soil dataset 2002, described as Silt Mont Cenis (*Limon Silteux*). The selected soils contain retention data points from drying and wetting experiments, and also conductivity data. These datasets show meaningful hysteretic behavior between the drying and wetting experiment data.

For retention data [h, θ] from the wetting experiment, water content values correspond to pressure head values lower than those in the drying experiment. For the conductivity data, the [K, θ] data, no meaningful difference between wetting and drying experiments was observed.

To evaluate the hysteretic behavior, a fitting process is developed to calibrate the retention function (Eq. 43) model. Simultaneously, the conductivity function (Eq. 49) is also calibrated. The simultaneous fitting for retention and conductivity functions is a standard approach (Mertens et al., 2006). The simultaneous calibration fits the parameters: b, α, n, θ_r, θ_s, K_s, and λ.

The logarithm transformation in base 10 is used on the conductivity data to account for the magnitude differences within it. Both retention and conductivity datasets are combined into one Of, and to assess the magnitude differences, a proper weighting method is required. The conductivity data, [$\log_{10}(K)$], are subjected to a weight of 0.1, while the

retention data (drying and wetting) keep the weight of 1. Further, the fitting process is performed for all soil datasets from UNSODA and the Mualem catalogue. The metric used to quantify the error is the RMSD.

2.8.3. A comparison between parameters: λ versus b

To evaluate the capability of the model to predict the conductivity function, analyzing the impact of parameter b over the modified VG conductivity function (Eq. 49), the author uses the same three soils used in the energy and approximation analysis, i.e., Loamy Sand, Silt Loam, and Silty Clay, from Rosetta, according to the 12 USDA soil texture classification. The Figures for the three soils are plotted, with multiple values for the parameters λ and b, showing the impact of both parameters on the shape of the function. The values of λ ranges from –1.0 to 4.0 and values of b from 0.1 to 2.0. All the tests are realized over the domain:

$$h \in \left[10^{-3}, 10^{3}\right] \text{ m} \qquad \text{(Eq. 63)}$$

A thousand points evenly spaced on a logarithmic scale (base 10) are sampled for the tests and RMSD calculation.

2.8.4. Preferential flow and solute transport

Another potential application of the model is the probabilistic quantification of the fraction of larger pores that remain water-filled, providing a basis for preferential flow and solute transport study.

To introduce the probabilistic approach to preferential flow, the author developed a theory in Appendix (section 5.1) for the breakthrough experiment equation, C_t/C_0, the related equation is Eq. 78. The value of b can also be estimated from transport experiment data. To test the probabilistic model under solute transport, data from Zurmühl (Zurmühl, 1998) was extracted from the images using the web tool WebPlotDigitizer. The extracted data correspond to Figure 5 in Zurmühl's work, where the author provides C_t/C_0 data per time. The experiment was realized with a cylindrical soil sample with length $L = 0.145$ m, and diameter, $D = 0.094$ m. Zurmühl provides data for 2 velocities: $q = 2.63 \text{ cm h}^{-1}$ and $q = 1.02 \text{ cm h}^{-1}$. Following Zurmühl's suggestion, the water content considered for the experiments are 0.2475 and 0.2210 $\text{m}^3\ \text{m}^{-3}$, respectively, which are the arithmetic means of measured values. The experimental data were filtered with respect to the rising concentration.

Zurmühl (1998) uses two different values of the parameter α, fixing the other retention parameters, to quantify the hysteretic characteristic between drying and wetting experiment data. Using both wetting and drying equations, the value of parameter b is also fitted based on drying and wetting scenarios.

The evaluation was conducted by fitting b for the Eq. 78, using data points [C_t/C_0; time]. Again, the metric used to assess the fitting accuracy is the RMSD between the predicted and measured data.

2.8.5. Physical interpretation of the b parameter

The interpretation of the probability of the back-transformation proposed is evaluated. For the discussion, the soil studied by Zurmühl (1998) is used again. The fitted b parameters described in the preferential flow section 2.8.4, are used in this analysis.

2.8.6. Configurational entropy favoring a mixture of filled and unfilled pores

A brief discussion about the findings of entropy configuration tending to filled and unfilled pores (Eq. 59 and 60) are realized. The calibrated models using Zurmühl datasets are used for the analysis of the configurational entropy tendency.

2.8.7. Brooks–Corey analytical solution test

Considering the pore size distribution extracted from the Brooks-Corey retention function, BC, (Brooks and Corey, 1964), the derivation of the retention function becomes straightforward. The linear relationship between the pressure head and the energy provides an analytical retention model. The development of the model is available in the Appendix, Section 5.2.

To evaluate the modified SP Brooks-Corey model, a brief discussion is provided about the impact of the parameter $b > 0$. The test is done over soil used in Vereecken et al. (2007), with parameters available in Table 2, where θ_s is the saturated water content [–], θ_r is the residual water content [–], η is a fitting parameter, and α^* is a fitting parameter [m^{-1}].

Table 2– Brooks-Corey parameters, from Vereecken et al. (2007), to evaluate the Brooks-Corey SP implementation.

θ_S	θ_r	α^* [m^{-1}]	η
0.410	0.057	17.700	1.070

The evaluation and discussion of this section are available in Appendix, Section 5.2.1.

3. RESULTS

3.1. Differences between approximations and energy conversions

A key simplification used to obtain an analytical formulation is the effective energy representation (Eq. 32), therefore, its consequences require evaluation. The saturation functions are plotted in Figure 2, for soils: Loamy Sand, Silt Loam, and Silty Clay, according to USDA soil classification with multiple values for parameter b. The dashed line represents the numerical solution using the capillary assumption and e_w (Eq. 28). The continuous lines are the functions using e_{eff} (Eq. 41). The colors represent different values of the parameter b. The case where $b = 0$ is represented by the blue continuous line, which is the same as the traditional VG retention function. The main visible impact of $b > 0$ over the retention function is the tendency to distance the retention function over

the x axis, leading to a smaller value of h (higher value of ψ). For small values of b, we notice a discrepancy between the value and shape of the function using e_w and e_{eff}. The RMSD of the difference between the formulations containing e_w and e_{eff} can be seen in Table 3. The highest value for the RMSD in Table 3 is 0.1362 for Silty clay soil with $b = 0.1$. The average RMSD is 0.05. Graphically, the shape differences between dashed and continuous curves of the same color are small, although there is a significant offset, the difference is not linearly related, as observed in Eq. 30 and Eq. 32.

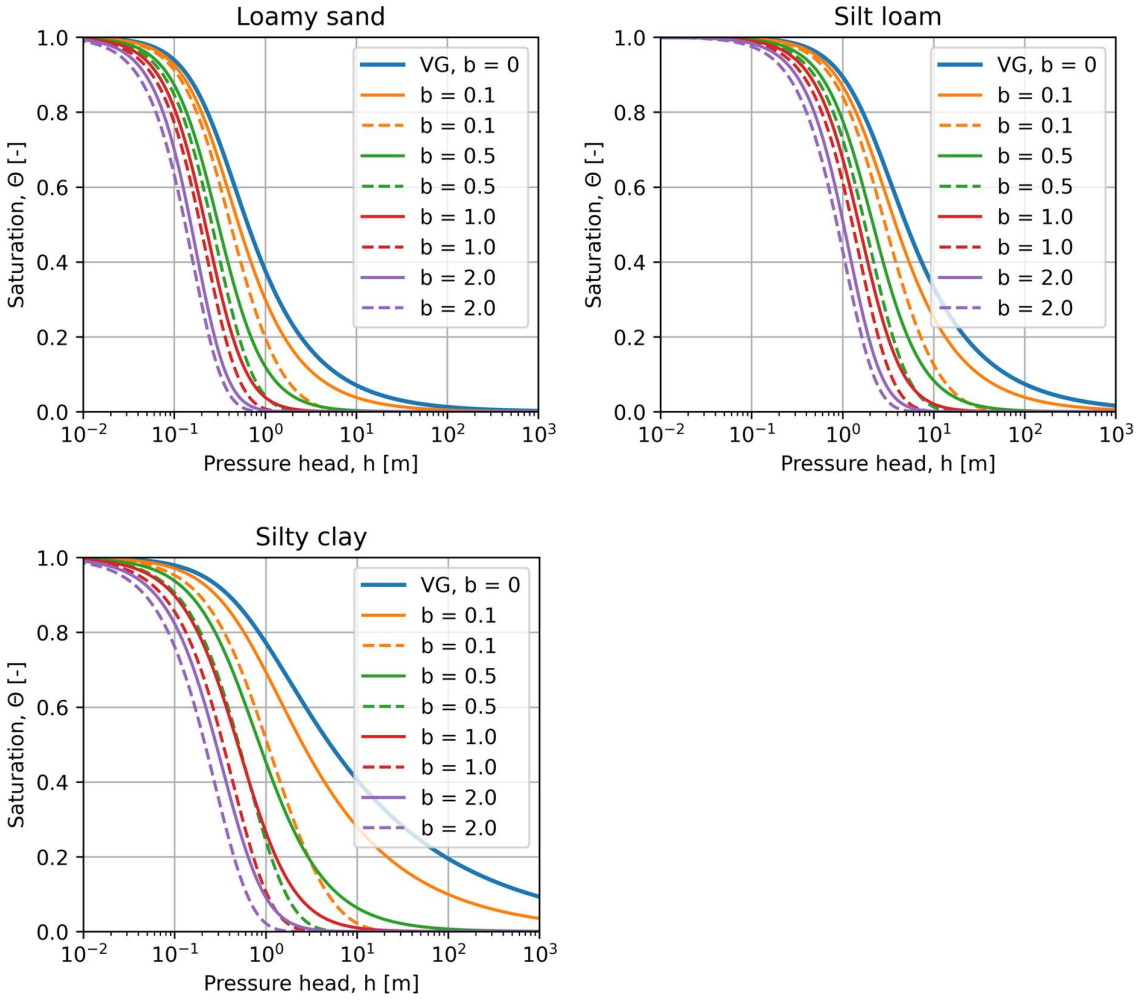


Figure 2 – Retention functions for three soils: Loamy Sand, Silt Loam, and Silty Clay, according to USDA soil texture classification. The dashed line represents the numerical solution of the retention function with energy proportional to pressure head, for $b > 0$, and the continuous line represents the retention function with closed-form and effective energy formulation. The VG continuous function represents the Van Genuchten model with $b = 0$.

549 Table 3 – Table containing the distances as root mean square distance (RMSD)
550 between retention functions with energy proportional to pressure head and
551 the effective energy formulation.

Soil	b value [–]	θ RMSD [$m^3\ m^{-3}$]
Loamy sand	0.1	0.0432
Loamy sand	0.5	0.0335
Loamy sand	1.0	0.0253
Loamy sand	2.0	0.0247
Silt loam	0.1	0.0532
Silt loam	0.5	0.0405
Silt loam	1.0	0.0305
Silt loam	2.0	0.0279
Silty clay	0.1	0.1362
Silty clay	0.5	0.0863
Silty clay	1.0	0.0613
Silty clay	2.0	0.0449

552

553 The approximation of the incomplete beta function was used in Eq. 48, to obtain an
554 analytical expression for K_{rel}. The RMSD values between the approximate and non-
555 approximate K_{rel} formulations, for different values of b, are presented in Table 4. The
556 maximum RMSD value was 0.0868, obtained for Silt loam at $b = 2.0$, while the mean
557 RMSD over all evaluated cases is 0.046. The magnitude of the approximation error
558 systematically increases as the value of b also increases; this pattern is observable in all
559 three soils. At $b = 0.1$, the RMSD values remained below 0.009 for all soils, whereas at
560 $b = 2.0$ it ranged from 0.0808 to 0.0868. The analytical approximation decreases the
561 RMSD value as b tends to zero.

562 Table 4 – Table containing the distances between relative conductivity functions, K_{rel},
563 for the analytical incomplete beta function, and approximated formulation.

Soil	b value [–]	K_{rel} RMSD [–]
Loamy sand	0.1	0.0087
Loamy sand	0.5	0.0351
Loamy sand	1.0	0.0573
Loamy sand	2.0	0.0855
Silt loam	0.1	0.0088
Silt loam	0.5	0.0355
Silt loam	1.0	0.0580
Silt loam	2.0	0.0868
Silty clay	0.1	0.0083
Silty clay	0.5	0.0332
Silty clay	1.0	0.0541
Silty clay	2.0	0.0808

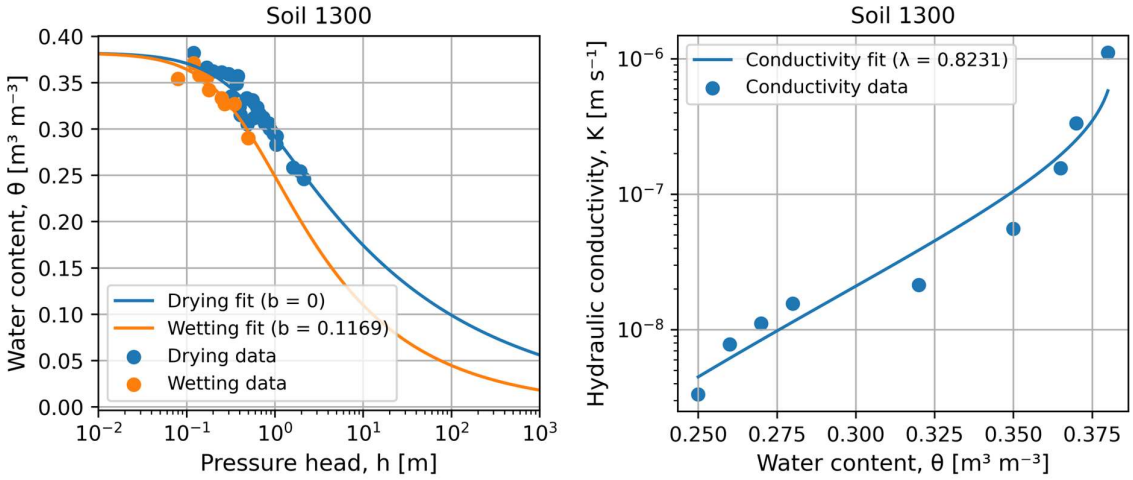
564

3.2. Retention and hydraulic conductivity evaluation VGM

Figure 3 presents the calibrated retention functions on the left (Eq. 43), and the corresponding conductivity functions on the right (Eq. 49), for four soil experimental datasets: 1300, 2002, 2020, 4870. Each soil dataset contains simultaneously: conductivity points $[K, \theta]$, and retention points $[h, \theta]$, obtained through wetting and drying scenarios. Experimental data are represented by the dots in the image, while the continuous lines represent the calibrated model; the wetting data and retention model are in orange, while the drying data and calibrated model are in blue. All calibrated retention models for the drying scenario use a fixed $b = 0$, while the models fitted to the wetting data and retention model possess a fitted value for $b > 0$. The conductivity model also uses the same value of b for the wetting scenario, following the proposed formulation observed in Eq. 49.

The fitted results show a consistent relationship between the magnitude of b and the observed wetting/drying separation. Table 5 contains the fitted parameters for soils 1300, 2002, 2020, and 4870. Soil 2020, in which the drying and wetting retention curves are relatively close, resulted in the smallest fitted value ($b = 0.0363$). In comparison, soils 1300, 2002, and 4870 exhibit progressively greater separation between the wetting and drying curves, with fitted b values: 0.1169, 0.1318, and 0.1530, respectively.

The RMSD values between measured and fitted retention data are presented in Table 6. Considering the retention data, including both wetting and drying data, the RMSD ranges from 0.007 to $0.021\ \mathrm{m^3 m^{-3}}$, while the individual wetting and drying branches show RMSD values between 0.003 and $0.026\ \mathrm{m^3 m^{-3}}$ respectively. The $\log_{10}(K)$ RMSD ranges from 0.117 to 0.216.



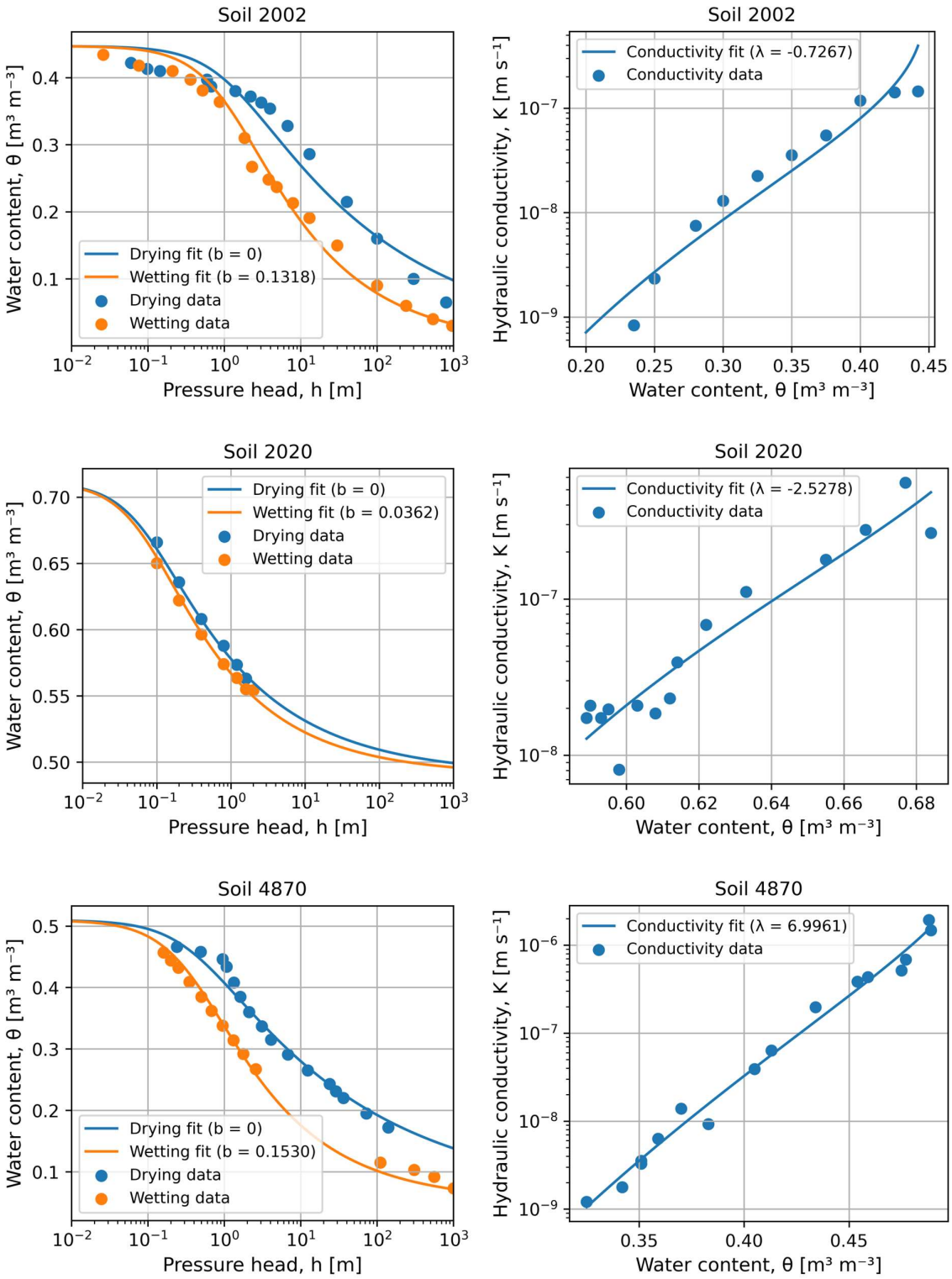


Figure 3 – Fitted retention and conductivity functions for soils: 1300, 2002, 2020, 4870.

Table 5 – Table containing the fitted parameters for soils: 1300, 2002, 2020, 4870, according to the introduced formulation.

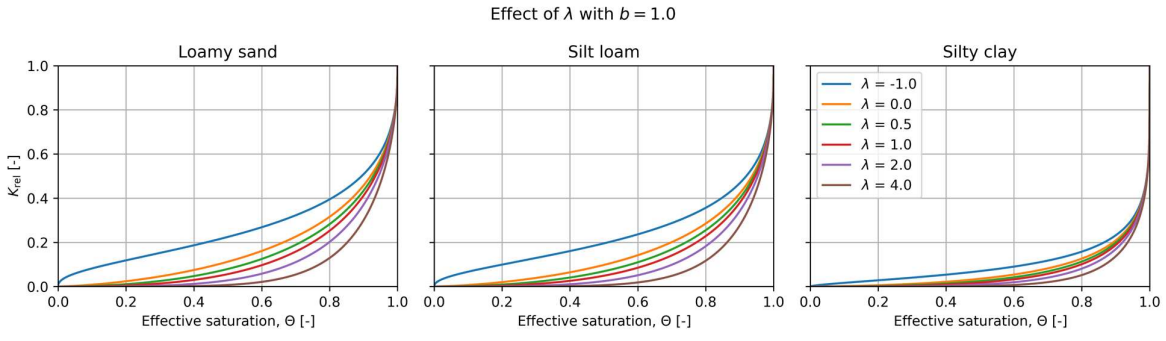
Fitted parameters	Soil			
	1300	2002	2020	4870
θ_r [m^3m^{-3}]	$1.326 \cdot 10^{-10}$	$7.339 \cdot 10^{-18}$	$4.906 \cdot 10^{-1}$	$5.149 \cdot 10^{-2}$
θ_s [m^3m^{-3}]	$3.820 \cdot 10^{-1}$	$4.470 \cdot 10^{-1}$	$7.107 \cdot 10^{-1}$	$5.095 \cdot 10^{-1}$
α [m^{-1}]	2.339	$9.253 \cdot 10^{-1}$	$1.543 \cdot 10^{+1}$	2.642
n [–]	1.247	1.223	1.335	1.211
b [–]	$1.169 \cdot 10^{-1}$	$1.318 \cdot 10^{-1}$	$3.625 \cdot 10^{-2}$	$1.530 \cdot 10^{-1}$
λ [–]	$8.231 \cdot 10^{-1}$	$-7.267 \cdot 10^{-1}$	–2.528	6.996
Ks [$m\ s^{-1}$]	$1.880 \cdot 10^{-6}$	$1.887 \cdot 10^{-6}$	$6.858 \cdot 10^{-6}$	$2.473 \cdot 10^{-5}$

Table 6 – Fitted parameter errors, expressed as values of RMSD, for soils: 1300, 2002, 2020, 4870.

	Soil – RMSD			
	1300	2002	2020	4870
Dry θ [$m^3\ m^{-3}$]	0.010	0.026	0.010	0.014
Wet θ [$m^3\ m^{-3}$]	0.008	0.015	0.003	0.011
Wet θ + Dry θ [$m^3\ m^{-3}$]	0.009	0.021	0.007	0.013
log10(K) [–]	0.184	0.216	0.168	0.117

3.3. Visual comparison between parameters b and λ

Figure 4 presents the relative hydraulic conductivity functions for three representative soil textural classes, Loamy Sand, Silt Loam, and Silty Clay, according to USDA classification. The upper panels show the effect of varying λ at fixed $b = 1.0$, and the lower panels show the effect of varying b at fixed $\lambda = 0.5$. Both parameters modify the curvature of the conductivity function, mostly at intermediate effective saturation. Their effects are qualitatively similar, but are inversely correlated: increasing λ decreases K_{rel} at a given Θ, and increasing b increases K_{rel}.



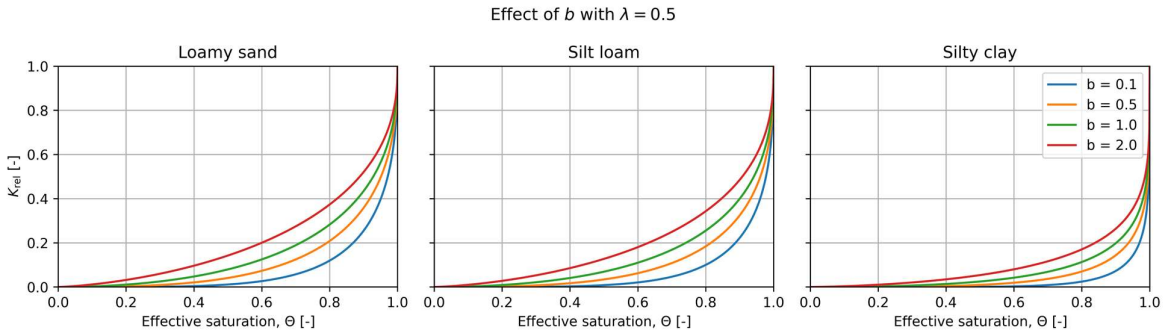


Figure 4 – Conductivity curves as a function of saturation, for the three USDA soils: Loamy sand, Silt loam, and Silty clay. The upper panels show the impact of changing the values for parameter λ, while the lower panels illustrate the impact of different values for parameter b.

3.4. Solute transport and preferential flow evaluation

Figure 5 illustrates an extension of the proposed statistical pore-occupancy framework to solute transport. The breakthrough-curve formulation developed in the Appendix combines the probability distribution of occupied pore states with the pore-dependent water velocity, using the same parameter b to influence the distribution of pore transport velocities. The statistical formulation can quantify transport processes, in which larger pores lead to faster solute transport. The fitted breakthrough curves reproduce the measured data provided by Zurmühl (1998), for both evaluated fluxes. Table 7 provides the fitted parameters and the RMSD values of this fitting procedure. The RMSD values are 0.018 and 0.016 for q=1.02 and 2.63 $\mathrm{cm\,h^{-1}}$, respectively. The corresponding fitted b values were 1.422 and 2.050. Zurmühl (1998) also provides the parameters for wetting and drying retention functions. Using both datasets, we fit $b = 1.191$. Interestingly, for Zurmühl soil, the value of b for the quasi-static case is smaller than that for the steady-state flow case.

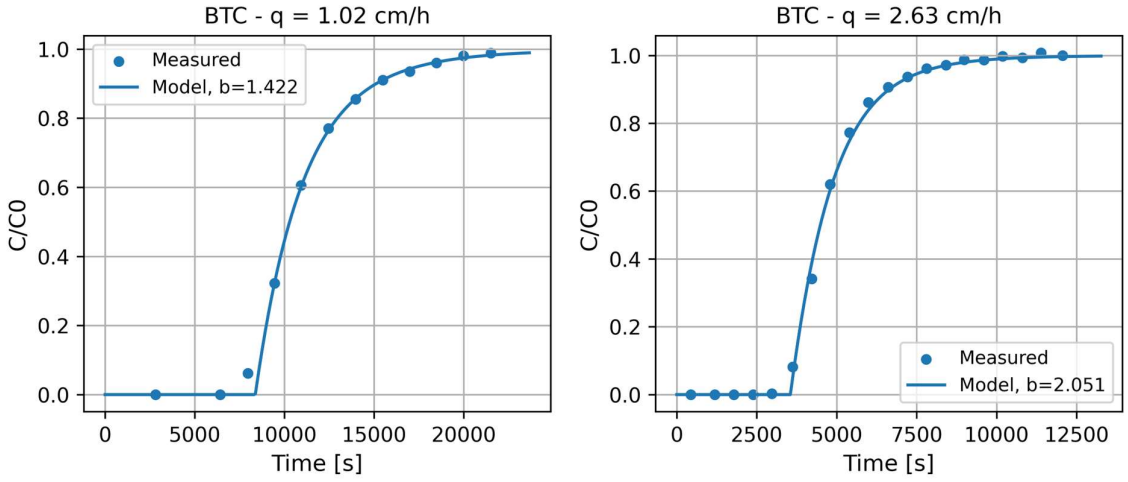


Figure 5 – Breakthrough curves (BTC) using the proposed breakthrough curve function using the statistical physics formulation, for two fluxes.

Table 7 – Table contains the errors (RMSD) for the breakthrough curve fitted functions (Figure 5).

h_{min} [m]	b [−]	RMSD [−]	h_{min} [m]	b [−]	RMSD [−]
Flux=1.02 [cm h^{-1}]			Flux=2.63 [cm h^{-1}]		
0.231	1.422	0.018	0.196	2.050	0.016

3.5. Configurational entropy of the filled pores

Figure 6 presents the configurational entropy (Eq. 59) as a function of h, with $b = 1.422$. The soil-water parameter dataset is available at Zurmühl (1998), for the flux rate $q = 1.02\ \mathrm{cm\ h^{-1}}$. For the binary pore representation, i.e., filled and unfilled, the configurational entropy is maximal at $\Theta = 0.5$. The retention contribution led to a maximal configurational entropy at $h = 0.190$ m.

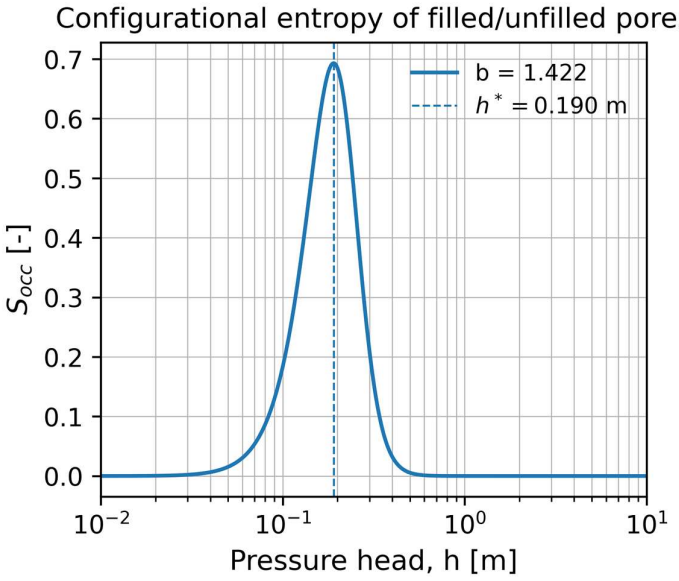


Figure 6 – Configurational entropy, S_{occ} [−], as a function of pressure head h [m], at flux rate $q = 1.02\ \mathrm{cm\ h^{-1}}$.

3.6. Retrieved pore-filling probabilities

The back–transformation provides a link between the fitted macroscopic parameter b and the statistical distribution of pore occupancy in the energy domain. The resulting b_{phys} varies with energy; its value at a particular state should not be interpreted as a single constant parameter for the entire distribution. For the two Zurmühl (1998) BTC experiments, the fitted effective values $b = 1.422$ and $b = 2.050$ correspond to $b_{phys} = 0.9195$ and 0.8735, respectively (Eq. 50), after considering the different hydraulic pressure states. Then, the pore-occupancy distribution may be expressed through $P_{VG}(h, b)$ in Eq. 58, which is a probability density with respect to pressure head. For the velocity $q =$

$1.02\ \mathrm{cm\ h^{-1}}$ case, evaluating the probability density near $h = 0.231\ \mathrm{m}$, leads to $P_{VG}(h_{min}) = 4.96\ \mathrm{m^{-1}}$. The integration over the interval $0.231 < h < 0.241\ \mathrm{m}$, and normalized over $\in [0; \infty)\ \mathrm{m}$, gives a dimensionless probability of 0.04611, which is approximately 4.6% of the pore-occupancy probability, considering the model-based inference is valid.

4. Discussion

4.1. Comparison with previous models and contribution of the framework

The contribution of the introduced framework is the explicit incorporation of probabilistic pore occupancy into conventional soil hydraulic functions. The statistical-physics approaches reviewed in the Introduction establish a basis for describing water occupancy and its relationship to macroscopic behaviour. Here, this description is embedded in the Van Genuchten–Mualem formulation through the parameter b, linking the changes in the retention and conductivity functions to an assumed distribution of occupied pore states. The traditional formulation is re-stablished at $b = 0$, allowing the effects of the introduced mechanism to be evaluated relative to the conventional model.

The applications demonstrate how this coupling can represent wetting and drying retention differences, while retaining a corresponding conductivity formulation (Figure 3, Tables 5 and 6). The extension to breakthrough curves provides an additional application of the occupancy framework to solute transport (Figure 5 and Table 7). The hydraulic and transport applications involved separate calibrations, establishing different values for b. The methodological contribution is a probabilistic description that can be evaluated using macroscopic measurements and used to derive conditional estimates of pore occupancy.

For comparison, Xu and Louge (2015) represented hysteresis through interactions among neighboring pores in an Ising formulation. Here, an effective parameter b embeds probabilistic pore occupancy directly in the van Genuchten–Mualem retention and conductivity functions.

4.2. Implications for retention, conductivity, and solute transport

The energy transformation made to achieve the algebraic retention function leads to a significant impact on the retention value prediction. For example, the RMSD of the retention function, resulting solely from the fitting process in Pinheiro et al., (2019), is around 0.02 and 0.03 $\mathrm{m^3\ m^{-3}}$, while the average RMSD in Table 3 is ~0.05 $\mathrm{m^3\ m^{-3}}$. On the other hand, although more tests are required, the shape differences due to the non-linearities of the conversion might not be significant in real-world applications. To address these issues, the conversion presented in Section 2.5 was developed.

For $b = 0$, the developed retention model (Eq. 43) reduces to the traditional VGM retention function. The capillary bundle assumption, which states that the smaller-radius pores are preferentially filled with water (Mualem 1976b), is used as the reference configuration. In this study, the drying experimental data are assumed as the reference configuration ($b = 0$), implying that the minimum-radius pores are filled. Nonetheless, this ideal scenario has

limitations, as investigated by Gu and Bazant (2018), Jiang et al. (2026), and Wang et al. (2025).

The proposed retention formulation is able to represent hysteresis. The behaviour of the retention functions in Figure 3 is consistent with the interpretation of b, as a measure of pore-filling configuration. Within the proposed pore-energy framework, increasing b increases the statistical distribution of water occupancy over the available pore-energy states, while shifting the retention relation away from the preferential occupation of the lowest-energy states.

The RMSD values from Table 6 show that the introduced b parameters allow the simultaneous fitting of conductivity parameters, the retention function, and the respective hysteretic displacement. For comparison, Inforsato et al. (2020) fitted the VG retention and conductivity functions, using three soil datasets from Mualem's catalogue; the average RMSD for the retention functions was $0.091\ \mathrm{m^3 m^{-3}}$, and the average of $\log_{10}(K)$ was 0.29, which are the same order of magnitude as the proposed model predictions.

A direct comparison between the predictability of the introduced model and the conventional VG fitting is not straightforward: the calibration of the introduced model simultaneously constrains drying retention, wetting retention, and hydraulic conductivity. In addition, the conductivity residuals in $\log_{10}(K)$ were assigned a weight of 0.1 relative to the retention residuals, giving the retention observations a larger contribution to the objective function, while there is no standard procedure for weighting $\log_{10}(K)$ (Mertens et al., 2006; Peters, 2013). Instead of independent optimizations, the fitted parameter set presents a combined optimized conductivity and retention model, including the hysteretic behaviour. In the proposed model, b not only provides another degree of freedom, but also introduces pore-scale mechanics that can be measured on a macroscopic scale, which is based on the statistical distribution of water in the pore.

Different combinations of b and λ may partially compensate for each other and produce similar conductivity curves. This indicates a high parameter correlation interaction between b and λ when using conductivity data alone. Nevertheless, the two parameters are not algebraically equivalent, and b also impacts the retention function.

For the breakthrough curves, the 2 different fitted b values for the same soil with 2 different saturation degrees (Figure 5), raises the possibility that b is not necessarily an invariant soil property at multiple saturation degree levels. In the present formulation, b is an effective parameter describing the statistical redistribution of water among available pore-energy states. The fitted values suggest that the effective occupancy weighting may vary with hydraulic state, depending on the saturation degree. Furthermore, the hysteresis is fundamentally dependent on the previous state of the water distribution through the soil pores (Visintin, 1994), therefore, the effective value of b might be significantly dependent on the saturation degree or the previous state of the water in the pores, leading to $b = b(\Theta)$. More dedicated experiments are necessary to validate the physical assumption of the model.

The S_{occ} reflects both the introduced retention function model and the configurational entropy. Under fixed water content and energetic constraints, configurational entropy may favor redistribution among accessible pore states. The configurational entropy is a consequence of the model assumption. On the other hand, local energy imbalances might

be the cause of this non-optimal state. A relevant consideration is that these two contributions alone (binary representation and retention function) are not enough to fully describe the pore occupancy state of the soil. Additional physical mechanics might influence occupation distribution, leading to different entropy behavior; other contributions may be due to gravitational potential, kinetic energy of water moving through the soil, and surface tension effects in laminar flow.

For the back-transformation, the results illustrate how the macroscopic retention relation can be used to infer the ensemble average state of the water in the soil. The parameter b is fitted and used for the effective–energy hydraulic formulation. The back-transformation expresses its weighting in terms of physical pore energy and may be used to obtain the corresponding pore occupancy probability distribution, under the proposed model's assumption.

The intended practical application of the proposed framework is a macro-to-micro procedure. The parameter b is not expected to be determined from direct observations of individual pores. Instead, conventional macroscopic measurements, such as soil-water retention, hydraulic conductivity, or transport data, are used to estimate b together with the corresponding hydraulic parameters. Once b and the macroscopic hydraulic state are known, the back-transformation can be applied to recover the physical-energy representation and the associated pore-occupancy probability distribution. Integration of this distribution over a selected pressure head interval provides the probability mass associated with that pore class, according to the introduced model. Hence, the framework uses quantities measurable at the macroscopic scale to infer statistical information about microscopic pore occupancy, without requiring direct observation of individual pore states.

4.3. Limitations and future work

The physical interpretation of the inferred occupancy distributions is conditional on the framework's assumptions. The cylindrical-pore representation and statistical weighting do not explicitly resolve pore-network connectivity. Although the formulation represents the measured wetting and drying branches, it does not provide a general description of scanning curves. Such an extension would require an evolution rule for b, that accounts for hydraulic history, including reversals between wetting and drying scenarios.

The effective-energy representation and the approximation used for hydraulic conductivity introduce differences from the corresponding reference formulations (Figure 2, Tables 3 and 4). Their consequences for simulated water flow and solute transport have not been evaluated here. Parameter estimation also requires further investigation: the opposing effects of b and λ on conductivity suggest potential compensation between these parameters (Figure 4). In the transport formulation, all water represented by the experimental water content is assumed to participate in transport, without explicitly distinguishing mobile and immobile water domains.

Future evaluation should combine retention, conductivity, and transport observations from the same samples across controlled saturation states and wetting and drying scenarios. Such measurements would allow tests of parameter transferability. Independent observations of water distribution among pore classes would provide a more direct test

of the inferred probabilities. These evaluations are needed to determine whether b can be treated as constant under specified conditions or requires an explicit dependence on hydraulic state and history.

The Python code used in this work is available at:

https://github.com/infoleon/probabilistic_pore_model

5. CONCLUSIONS

In this study, a framework with statistical physics principles was developed. To test the framework, a model based on the Van Genuchten-Mualem retention and conductivity functions was developed and analyzed, evidencing the model's capability to predict:

1. hysteretic behavior of retention functions,
2. solute breakthrough curves,
3. water-filled pore configuration state, conditioned on accepting the model assumption.

The newly introduced b parameter links these three applications through the proposed pore occupancy formulation.

The evidence shown allows us to conclude that the proposed framework, with the introduced soil hydraulic model, is capable of inferring the pore occupancy distribution.

Acknowledgements

This work was made possible thanks to the support of *Paciência de Laura* S.L.; the author is immensely grateful.

6. APPENDIX

6.1. Breakthrough Curve function definition

Here we develop the theory for the breakthrough curve considering the probabilistic model developed.

From Poiseuille (Bird et al., 2007), the proportion between the flux Q [$\mathrm{m^3\ s^{-1}}$] and the pore radius r [m] is

$$Q(r) \propto r^4 \tag{Eq. 64}$$

For the fluid velocity v [$\mathrm{m/s}$], the relationship becomes

$$v(r) \propto r^2 \tag{Eq. 65}$$

Given that $h \propto r^{-1}$, the v proportionality to h becomes

$$v(h) \propto \frac{1}{h^2} \quad \text{(Eq. 66)}$$

Which can be written as

$$v(h) = A(b) \cdot h^{-2} \quad \text{(Eq. 67)}$$

Here, $A(b)$ is a constant. From Zurmühl, (1998), the mean v, noted as $\overline{v}$ [m s^{-1}], is

$$\overline{v} = \frac{q}{\theta} \quad \text{(Eq. 68)}$$

q = flux density [m s^{-1}]

The mean velocity with respect to the probability distribution Eq. 39 is

$$\frac{q}{\theta} = \overline{v} = \int_{h_{\min}}^{h_{\max}} v(h,b)\, p_{tr}(h,b)\, dh \quad \text{(Eq. 69)}$$

where

$$p_{tr}(h,b) = \frac{P_{VG}(h,b)}{\int_{h_{\min}}^{h_{\max}} P_{VG}(h,b)\, dh} \quad \text{(Eq. 70)}$$

Substituting with Eq. 67

$$\frac{q}{\theta} = A(b) \cdot \int_{h_{\min}}^{h_{\max}} h^{-2} \cdot p_{tr}(h,b)\, dh \quad \text{(Eq. 71)}$$

Solving for $A(b)$ gives

$$A(b) = \frac{q}{\theta} \cdot \frac{\int_{h_{\min}}^{h_{\max}} P_{VG}(h,b)\, dh}{\int_{h_{\min}}^{h_{\max}} h^{-2} \cdot P_{VG}(h,b)\, dh} \quad \text{(Eq. 72)}$$

with

$$v(h,b) = A(b) \cdot h^{-2} \quad \text{(Eq. 73)}$$

Since the time [s] is

$$t = \frac{L}{v(h,b)} \quad \text{(Eq. 74)}$$

L = size of the soil sample under analysis [m]

Isolating the time [s], we achieve

$$t = \frac{L\theta}{q} \cdot h^2 \cdot \frac{\int_{h_{\min}}^{h_{\max}} h^{-2} \cdot P_{VG}(h,b)\, dh}{\int_{h_{\min}}^{h_{\max}} P_{VG}(h,b)\, dh} = \frac{L \cdot h^2}{A(b)} \quad \text{(Eq. 75)}$$

Isolating h

$$h(t,b) = \sqrt{\frac{A(b) \cdot t}{L}} \quad \text{(Eq. 76)}$$

Considering concentration as C [kg m^{-3}], the input concentration as C_0 and output concentration C_t; the breakthrough equation, defined as C_t/C_0 [–], is calculated by weighting the concentrations by the distribution p_{tr}, resulting in

$$\frac{C_t(t,b)}{C_0} = \frac{\int_{h_{\min}}^{h(t,b)} v(h,b)\cdot p_{tr}(h,b)\,dh}{\int_{h_{\min}}^{h_{\max}} v(h,b)\cdot p_{tr}(h,b)\,dh} \qquad \text{(Eq. 77)}$$

Using the Eq. 67 to make h explicit by substituting v, and canceling the normalization integral,

$$\frac{C_t(t,b)}{C_0} = \frac{\int_{h_{\min}}^{h(t,b)} h^{-2}\cdot P_{VG}(h,b)\,dh}{\int_{h_{\min}}^{h_{\max}} h^{-2}\cdot P_{VG}(h,b)\,dh} \qquad \text{(Eq. 78)}$$

With t_{min} and t_{max} as

$$t_{\min} = \frac{L\cdot {h_{\min}}^2}{A(b)} \qquad t_{\max} = \frac{L\cdot {h_{\max}}^2}{A(b)} \qquad \text{(Eq. 79)}$$

for $t < t_{min}$, $C_t/C_0 = 0$.

Eq. 78 describes the normalized outlet concentration, C_t/C_0. The formulation assumes that all water represented by the experimental volumetric water content (θ) participates in solute transport. For each trial b, the lower bound h_{min} is calculated from the retention relation at the experimental θ, representing the largest included water–filled pore. The upper bound, h_{max}, represents the smallest included pore and is taken as infinity or a prescribed finite cutoff.

6.2. Statistical physics formulation for Brooks–Corey retention function

Here we define the Brooks-Corey, BC, retention function (Brooks and Corey, 1964), without using the energy transformation. The Brooks-Corey retention function is defined as

$$\Theta_{BC}(h) = \begin{cases} 1, & h \le 1/\alpha^* \\ \left(\alpha^* h\right)^{-\eta}, & h > 1/\alpha^* \end{cases} \qquad \text{(Eq. 80)}$$

where

$$\Theta(\theta) = \frac{\theta - \theta_r}{\theta_s - \theta_r} \qquad \text{(Eq. 81)}$$

α^* = fitting parameter [m^{-1}]

η = fitting parameter [–], with $\eta > 0$

The $C(h)$ from Eq. 12, for the BC function becomes

$$C_{BC}(h) = -\frac{d\theta}{dh} = (\theta_s - \theta_r)\eta\alpha^*\left(\alpha^* h\right)^{-\eta-1} \qquad \text{(Eq. 82)}$$

With the BC model, e_w is used

$$e_w(h) = \rho_w\cdot V_0\cdot g\cdot h\,, \qquad b = \frac{\beta\cdot\rho_w\cdot V_0\cdot g}{\alpha^*} \qquad \text{(Eq. 83)}$$

Substituting into the Boltzmann probability distribution, Eq. 20

$$P_{BC}(h,b)=\frac{\eta\alpha^{*}\left(\alpha^{*}h\right)^{-\eta-1}\cdot\exp\left(-b\alpha^{*}h\right)}{\int_{1/\alpha^{*}}^{\infty}\eta\alpha^{*}\left(\alpha^{*}h\right)^{-\eta-1}\cdot\exp\left(-b\cdot\alpha^{*}\cdot h\right)\,dh} \quad \text{(Eq. 84)}$$

Leading to

$$P_{BC}(h,b)=\frac{\alpha^{*}\left(\alpha^{*}h\right)^{-\eta-1}\exp\left(-b\alpha^{*}h\right)}{b^{\eta}\Gamma\left(-\eta,b\right)} \quad \text{(Eq. 85)}$$

Then, integrating P_{BC} leads to BC saturation,

$$\Theta_{BC}(h,b)=\int_{h}^{\infty}P_{BC}(h,b)\,dh \quad \text{(Eq. 86)}$$

After integration

$$\Theta_{BC}(h)=\begin{cases}1, & h\le\dfrac{1}{\alpha^{*}}\\ \dfrac{\Gamma\left(-\eta,\mathrm{b}\,\alpha^{*}h\right)}{\Gamma\left(-\eta,b\right)}, & h>\dfrac{1}{\alpha^{*}}\end{cases} \quad \text{(Eq. 87)}$$

6.2.1. Testing the mechanism incorporated into the Brooks–Corey model

Figure 7 shows the Brooks-Corey retention function obtained with the statistical pore-occupancy formulation for different values of b. The case $b=0$ corresponds to the original Brooks-Corey retention function, whereas increasing b progressively increases the separation from this reference curve after air entry, resulting in lower water content at a given pressure head and a steeper transition toward the residual water content. An important characteristic of the Brooks-Corey formulation is that all curves remain identical in the saturated region and intersect at the same air-entry pressure, $h=1/\alpha^{*}$. This occurs because the statistical weighting modifies only the post-air-entry branch of the retention function, while the air-entry parameter α^{*} itself remains unchanged. Therefore, b controls the redistribution of water within the draining pore domain without modifying the pressure at which desaturation begins.

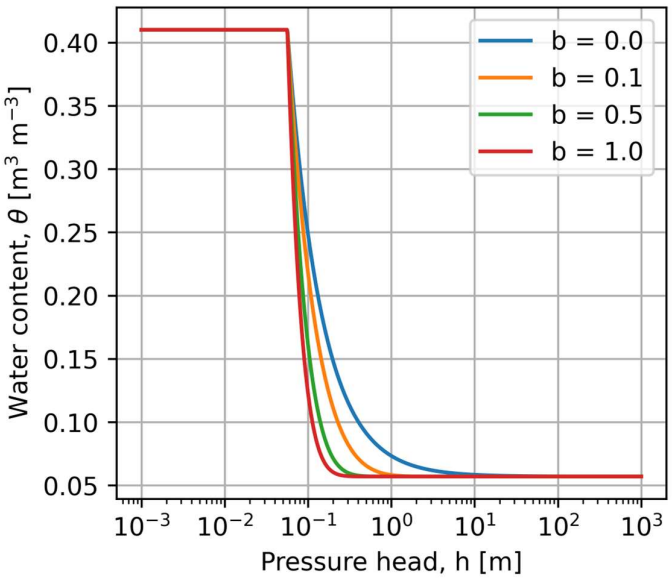


Figure 7 – Statistical physics formulation of Brooks–Corey retention function, with multiple values of b parameter.

7. REFERENCES

Bird, R. B., Stewart, W. E., & Lightfoot, E. N. (2007). *Transport phenomena* (Revised ed). Wiley.

Blundell, S. J., & Blundell, K. M. (2009). *Concepts in Thermal Physics* (2nd ed.). Oxford University PressOxford. https://doi.org/10.1093/acprof:oso/9780199562091.001.0001

Branch, M. A., Coleman, T. F., & Li, Y. (1999). A Subspace, Interior, and Conjugate Gradient Method for Large-Scale Bound-Constrained Minimization Problems. *SIAM Journal on Scientific Computing*, *21*(1), 1–23. https://doi.org/10.1137/S1064827595289108

Brooks, R. H., & Corey, A. T. (1964). Hydraulic properties of porous media. *Hydrology Papers, Colorado State University. Fort Collins CO*, *3*(3), 27–27.

Celia, M. A., Bouloutas, E. T., & Zarba, R. L. (1990). A general mass-conservative numerical solution for the unsaturated flow equation. *Water Resources Research*, *26*(7), 1483–1496. https://doi.org/10.1029/WR026i007p01483

Childs, E. C., & Collis-George, N. (1950). The permeability of porous materials. *Proceedings of the Royal Society of London. Series A. Mathematical and Physical Sciences*, *201*(1066), 392–405. https://doi.org/10.1098/rspa.1950.0068

De Jong van Lier, Q. (2017). Field capacity, a valid upper limit of crop available water? *Agricultural Water Management*, *193*, 214–220. https://doi.org/10.1016/j.agwat.2017.08.017

Didonato, A. R., & Morris, A. H. (1992). Algorithm 708: Significant digit computation of the incomplete beta function ratios. *ACM Transactions on Mathematical Software*, *18*(3), 360–373. https://doi.org/10.1145/131766.131776

Dourado Neto, D., De Jong Van Lier, Q., Van Genuchten, M. Th., Reichardt, K., Metselaar, K., & Nielsen, D. R. (2011). Alternative Analytical Expressions for the General van Genuchten–Mualem and van Genuchten–Burdine Hydraulic Conductivity Models. *Vadose Zone Journal*, *10*(2), 618–623. https://doi.org/10.2136/vzj2009.0191

Durner, W. (1994). Hydraulic conductivity estimation for soils with heterogeneous pore structure. *Water Resources Research*, *30*(2), 211–223. https://doi.org/10.1029/93WR02676

Emerman, S. H. (1995). The tipping bucket equations as a model for macropore flow. *Journal of Hydrology*, *171*(1–2), 23–47. https://doi.org/10.1016/0022-1694(95)02735-8

Fredlund, D. G., & Xing, A. (1994). *Equations for the soil-water characteristic curve.* (Geotech. J., Vol. 31, pp. 521–532). www.nrcresearchpress.com

Gerke, H. H., & Van Genuchten, M. T. (1993). A dual-porosity model for simulating the preferential movement of water and solutes in structured porous media. *Water Resources Research*, *29*(2), 305–319. https://doi.org/10.1029/92WR02339

Grant, C. D., Groenevelt, P. H., & Robinson, N. I. (2010). Application of the Groenevelt-Grant soil water retention model to predict the hydraulic conductivity. *Australian Journal of Soil Research*, *48*(5), 447–458. https://doi.org/10.1071/SR09198

Groenevelt, P. H., & Grant, C. D. (2004). A new model for the soil-water retention curve that solves the problem of residual water contents. *European Journal of Soil Science*, *55*(3), 479–485. https://doi.org/10.1111/j.1365-2389.2004.00617.x

Gu, Z., & Bazant, M. Z. (2018). *Microscopic theory of capillary pressure hysteresis based on pore-space accessibility and radius-resolved saturation*. arXiv. https://doi.org/10.48550/ARXIV.1808.09804

Hansen, A., Flekkøy, E. G., Sinha, S., & Slotte, P. A. (2023). A statistical mechanics framework for immiscible and incompressible two-phase flow in porous media. *Advances in Water Resources*, *171*, 104336. https://doi.org/10.1016/j.advwatres.2022.104336

Inforsato, L., & de Jong van Lier, Q. (2021). Polynomial functions to predict flux-based field capacity from soil hydraulic parameters. *Geoderma*, *404*, 115308. https://doi.org/10.1016/j.geoderma.2021.115308

Inforsato, L., de Jong van Lier, Q., & Pinheiro, E. A. R. (2020). An extension of water retention and conductivity functions to dryness. *Soil Science Society of America Journal*, *84*(1). https://doi.org/10.1002/saj2.20014

Jaynes, E. T. (1957). Information Theory and Statistical Mechanics. *Physical Review*, *106*(4), 620–630. https://doi.org/10.1103/PhysRev.106.620

Jiang, Z., Leung, A. K., & Liu, J. (2026). Quantifying pore-scale heterogeneity of drying and wetting soil water retention behavior using X-ray computed tomography. *Canadian Geotechnical Journal*, *63*, 1–16. https://doi.org/10.1139/cgj-2025-0203

Köhne, J. M., Köhne, S., & Gerke, H. H. (2002). Estimating the hydraulic functions of dual-permeability models from bulk soil data. *Water Resources Research*, *38*(7). https://doi.org/10.1029/2001WR000492

Kool, J. B., & Parker, J. C. (1987). Development and evaluation of closed-form expressions for hysteretic soil hydraulic properties. *Water Resources Research*, *23*(1), 105–114. https://doi.org/10.1029/WR023i001p00105

Lu, N., & Khorshidi, M. (2015). Mechanisms for Soil-Water Retention and Hysteresis at High Suction Range. *Journal of Geotechnical and Geoenvironmental Engineering*, *141*(8), 04015032. https://doi.org/10.1061/(ASCE)GT.1943-5606.0001325

Mertens, J., Stenger, R., & Barkle, G. F. (2006). Multiobjective Inverse Modeling for Soil Parameter Estimation and Model Verification. *Vadose Zone Journal*, *5*(3), 917–933. https://doi.org/10.2136/vzj2005.0117

Minasny, B., Bandai, T., Ghezzehei, T. A., Huang, Y.-C., Ma, Y., McBratney, A. B., Ng, W., Norouzi, S., Padarian, J., Rudiyanto, Sharififar, A., Styc, Q., & Widyastuti, M. (2024). Soil Science-Informed Machine Learning. *Geoderma*, *452*, 117094. https://doi.org/10.1016/j.geoderma.2024.117094

Mualem, Y. (1974). A conceptual model of hysteresis. *Water Resources Research*, *10*(3), 514–520. https://doi.org/10.1029/WR010i003p00514

Mualem, Y. (1976a). A catalogue of the hydraulic properties of unsaturated soils. *Research Project No.442*, 100 p.-100 p.

Mualem, Y. (1976b). A new model for predicting the hydraulic conductivity of unsaturated porous media. *Water Resources Research*, *12*(3), 513–522. https://doi.org/10.1029/WR012i003p00513

Nemes, A., Schaap, M., & Leij, F. (n.d.). *The UNSODA Unsaturated Soil Hydraulic Database Version 2.0*.

Nimmo, J. R., Herkelrath, W. N., & Laguna Luna, A. M. (2007). Physically Based Estimation of Soil Water Retention from Textural Data: General Framework, New Models, and Streamlined Existing Models. *Vadose Zone Journal*, *6*(4), 766–773. https://doi.org/10.2136/vzj2007.0019

Or, D., & Tuller, M. (2023). Capillarity. In *Encyclopedia of Soils in the Environment* (pp. 225–239). Elsevier. https://doi.org/10.1016/B978-0-12-822974-3.00115-4

Padarian, J., Minasny, B., & McBratney, A. B. (2020). Machine learning and soil sciences: A review aided by machine learning tools. *SOIL*, *6*(1), 35–52. https://doi.org/10.5194/soil-6-35-2020

Peters, A. (2013). Simple consistent models for water retention and hydraulic conductivity in the complete moisture range. *Water Resources Research*, *49*(10), 6765–6780. https://doi.org/10.1002/wrcr.20548

Pinheiro, E. A. R., de Jong van Lier, Q., Inforsato, L., & Šimůnek, J. (2019). Measuring full-range soil hydraulic properties for the prediction of crop water availability using gamma-ray attenuation and inverse modeling. *Agricultural Water Management*, *216*. https://doi.org/10.1016/j.agwat.2019.01.029

Puckett, J. G., & Daniels, K. E. (2013). Equilibrating Temperature-like Variables in Jammed Granular Subsystems. *Physical Review Letters*, *110*(5), 058001. https://doi.org/10.1103/PhysRevLett.110.058001

Rigon, R. (2026). *The Statistical physics of unsaturated soil water: Kinetic theory and non-commutative pore water dynamics*. arXiv. https://doi.org/10.48550/ARXIV.2607.09416

Ryo, M. (2022). Explainable artificial intelligence and interpretable machine learning for agricultural data analysis. *Artificial Intelligence in Agriculture*, *6*, 257–265. https://doi.org/10.1016/j.aiia.2022.11.003

Schaap, M. G., Leij, F. J., & Van Genuchten, M. T. (2001). Rosetta: A computer program for estimating soil hydraulic parameters with hierarchical pedotransfer functions. *Journal of Hydrology*, *251*(3–4), 163–176. https://doi.org/10.1016/S0022-1694(01)00466-8

Schroeder, D. V. (2021). *An Introduction to Thermal Physics* (1st ed.). Oxford University PressOxford. https://doi.org/10.1093/oso/9780192895547.001.0001

Siqveland, L. M., & Skjaeveland, S. M. (2021). Derivations of the Young-Laplace equation. *Capillarity*, *4*(2), 23–30. https://doi.org/10.46690/capi.2021.02.01

Turek, M. E., De Jong Van Lier, Q., & Armindo, R. A. (2022). Parameterizing field capacity as the upper limit of available water in bucket-type hydrological models. *Computers and Electronics in Agriculture*, *194*, 106801. https://doi.org/10.1016/j.compag.2022.106801

Van Genuchten, M. Th. (1980). A Closed-form Equation for Predicting the Hydraulic Conductivity of Unsaturated Soils. *Soil Science Society of America Journal*, *44*(5), 892–892. https://doi.org/10.2136/sssaj1980.03615995004400050002x

Vereecken, H., Kamai, T., Harter, T., Kasteel, R., Hopmans, J., & Vanderborght, J. (2007). Explaining soil moisture variability as a function of mean soil moisture: A stochastic unsaturated flow perspective. *Geophysical Research Letters*, *34*(22), 2007GL031813. https://doi.org/10.1029/2007GL031813

Vereecken, H., Schnepf, A., Hopmans, J. W., Javaux, M., Or, D., Roose, T., Vanderborght, J., Young, M. H., Amelung, W., Aitkenhead, M., Allison, S. D., Assouline, S., Baveye, P., Berli, M., Brüggemann, N., Finke, P., Flury, M., Gaiser, T., Govers, G., … Young, I. M. (2016). Modeling Soil Processes: Review, Key Challenges, and New Perspectives. *Vadose Zone Journal*, *15*(5), vzj2015.09.0131-vzj2015.09.0131. https://doi.org/10.2136/vzj2015.09.0131

Visintin, A. (1994). Hysteresis and Semigroups. In A. Visintin (Ed.), *Differential Models of Hysteresis* (pp. 211–256). Springer. https://doi.org/10.1007/978-3-662-11557-2_11

Wang, Y., Ma, R., & Vereecken, H. (2025). A Generalized Framework to Describe Unimodal and Bimodal Soil Hydraulic Properties Over Full Water Saturation Range. *Water Resources Research*, *61*(2), e2024WR038450. https://doi.org/10.1029/2024WR038450

Xu, J., & Louge, M. Y. (2015). Statistical mechanics of unsaturated porous media. *Physical Review E*, *92*(6), 062405. https://doi.org/10.1103/PhysRevE.92.062405

Yuan, Y., Xing, Y., Zheng, J., Li, Z., Yuan, H., Zhang, S., Zeng, Z., Xia, C., Tong, H., Kob, W., Zhang, J., & Wang, Y. (2021). Experimental Test of the Edwards Volume Ensemble for Tapped Granular Packings. *Physical Review Letters*, *127*(1), 018002. https://doi.org/10.1103/PhysRevLett.127.018002

Zehe, E., & Jackisch, C. (2016). A Lagrangian model for soil water dynamics during rainfall-driven conditions. *Hydrology and Earth System Sciences*, *20*(9), 3511–3526. https://doi.org/10.5194/hess-20-3511-2016

Zehe, E., Loritz, R., Edery, Y., & Berkowitz, B. (2021). Preferential pathways for fluid and solutes in heterogeneous groundwater systems: Self-organization, entropy, work. *Hydrology and Earth System Sciences*, *25*(10), 5337–5353. https://doi.org/10.5194/hess-25-5337-2021

Zehe, E., Loritz, R., Jackisch, C., Westhoff, M., Kleidon, A., Blume, T., Hassler, S. K., & Savenije, H. H. (2019). Energy states of soil water – a thermodynamic perspective on soil water dynamics and storage-controlled streamflow generation in different landscapes. *Hydrology and Earth System Sciences*, *23*(2), 971–987. https://doi.org/10.5194/hess-23-971-2019

Zhang, R., Song, C., Zhang, Z., Xie, J., Chen, T., & Xu, T. (2026). Machine learning for soil moisture analysis: A survey and emerging perspectives. *International Journal of Data Science and Analytics*, *21*(1), 66. https://doi.org/10.1007/s41060-025-00977-8

Zheng, W., Shen, C., Wang, L., & Jin, Y. (2020). An empirical soil water retention model based on probability laws for pore-size distribution. *Vadose Zone Journal*, *19*(1), e20065. https://doi.org/10.1002/vzj2.20065

Zurmühl, T. (1998). Capability of convection–dispersion transport models to predict transient water and solute movement in undisturbed soil columns. *Journal of Contaminant Hydrology*, *30*(1–2), 101–128. https://doi.org/10.1016/S0169-7722(97)00034-X